High-sensitive MXene and GST-based tunable refractive index sensor for the infrared and visible spectrum from multipurpose sensing applications

Kiran Khadka[1] and Bhishma Karki[2]

[1]Student, Department of Physics, Mahendra Morang Adarsh Multiple Campus, Tribhuvan University, Nepal
[2]Assistant Professor, Department of Physics, Tri-Chandra Multiple Campus, Tribhuvan University, Nepal

Corresponding Author
Kiran Khadka
Email: keerankc52@gmail.com
https://orcid.org/0009-0006-2811-583X

Received Date 06 February 2024 **Accepted Date** 20 August 2024 **Published Date** 1 September 2024

ABSTRACT

In this paper, a sensor with a multi-layered structure based on MXene and GST as an active plasmonic material is designed. The design is simulated in 2D. The design is a general sensor to detect refractive index from 1 to 1.14. Here, the design structure is arranged by placing the analyte on top. The middle metal layer is considered Ag/Au/Al/Cu to identify the effect of the metal layer on overall absorption and reflector. The GST layer is configured as a state material aGST and cGST, where the different properties of the states are considered for identification of the tunable behaviour of the structure. Optimisation and validation for parameters like height, width, and other metals, such as Ag/Au/Cu/Al processes, were conducted to ensure optimal device performance. The proposed refractive index sensor offers a high sensitivity variation ranging from 80 deg/RIU to 770 deg/RIU. Overall bandwidth and the resonating region are different for both phases of GST material. In other words, the proposed refractive index sensor can be used as a lab-on-chip biosensor.

KEYWORDS
GST, Metamaterials, MXene, Refractive index, Sensors, Tunability

INTRODUTION

It recently highlighted the growing significance of plasmonics in various technological applications, particularly in bridging the gap between electronics and optics (Zeng et al., 2014; Atabaki et al., 2018; Sun et al., 2015). Plasmonics offers the potential to manipulate electromagnetic fields at nanoscale levels, enabling faster speeds and broader bandwidth compared to traditional electronic devices. However, to fully capitalise on the advantages of plasmonics and address the challenges electronics face, further advancements are needed to create nanoscale devices with tunable and customisable characteristics (Chauhan et al., 2021). It will enable the complete transformation of the fundamental properties of photons and enhance reliability and functionality in applications such as imaging, communication, sensing, and medical technology (Aieta et al., 2017; Thomson et al., 2016; Rickman, 2014).

The term "metamaterials" originates from the Greek word "meta," meaning "beyond," indicating materials that possess properties beyond those of conventional materials. These materials exhibit unconventional characteristics derived from their structural arrangement rather than the properties of their components. V. G. Veselago's proposition in 1968 that materials combining metals and insulators are technically feasible marked a significant milestone in the development of metamaterials (Veselago, 1968). Since then, numerous researchers have explored the potential applications of metamaterials across various fields. Metamaterials can be categorised into different types based on their properties and applications, including electromagnetic metamaterials (Singha et al., 2015), chiral metamaterials (Jaggard et al., 1979), photonic metamaterials (Encyclopedia, 2022), tunable metamaterials, nonlinear metamaterials (Kivshar, 2009), and Frequency Selective Surface (FSS) based metamaterials (Khan and Eibert, 2018). The applications of metamaterials span a wide range of fields, including WMD (Weapons of Mass Destruction) detectors, invisible submarines, revolutionary electronics, light and sound filtering, biosensors, metamaterial absorbers, and metamaterial antennas (Rahmit, 2006; Caloza and Itoh, 2005). These materials offer unprecedented opportunities for innovation and technological advancement across multiple domains. Active plasmonic materials represent a cutting-edge class of materials with dynamic optical properties, offering many applications across various fields (Jiang et al., 2018). Their ability to manipulate light in real-time through absorption, reflection, and transmission changes makes them highly desirable for numerous technological advancements. One of the distinguishing features of active plasmonic materials is their capability to support plasmon resonances (Sbeah et al., 2023). These resonances, arising from collective electron oscillations within the material, strongly interact with incident light. The characteristics of these resonances, including their frequency and strength, can be tailored by adjusting parameters such as size, shape, composition, and the surrounding medium. For instance, metal nanoparticles can support plasmon resonances in the visible and near-infrared spectrum, while doped semiconductor nanoparticles can achieve resonances in the mid-infrared range (Stevenson et al., 2020). This flexibility in tuning plasmon resonances allows for precise control over the interaction between light and matter, enabling a wide range of applications. Active plasmonic materials can also serve as platforms for inducing phase transitions in response to external stimuli. For instance, applying an electric field to align liquid crystal materials can effectively tune the plasmon resonance of embedded metal nanoparticles. Upon removal of the electric field, the liquid crystal undergoes a phase transition, leading to alterations in its optical properties (Dickson et al., 2008). This dynamic behaviour enables the modulation of light-matter interactions, further expanding the utility of these materials. The potential applications of active plasmonic materials span diverse fields. In sensing applications, changes in plasmon resonance can be exploited to detect minute variations in the local environment, facilitating the detection of

specific molecules or monitoring temperature changes with high sensitivity. Moreover, in data storage and optical computing, the real-time manipulation of plasmon resonance offers opportunities for encoding and processing information efficiently (Tokarev et al., 2010). Overall, active plasmonic materials represent a versatile platform for developing next-generation technologies, with their dynamic optical properties opening doors to innovative solutions in sensing, data storage, optical computing, and beyond.

Surface plasmon resonance (SPR) sensors are highly significant inensing technology because they can detect changes in the refractive index near the sensor surface (Kaushik et al., 2019). Due to their remarkable sensitivity and high resolution, these sensors are widely utilised in various applications, including clinical diagnostics, environmental monitoring, and biochemical analysis (Lerner et al., 2014). SPR-based sensors typically operate on two primary configurations: the Kretschmann and Otto configurations. In the Kretschmann configuration, a thin metal film is deposited on a dielectric prism, allowing for the excitation of surface plasmons at the metal-dielectric interface. In the Otto configuration, the metal film is instead deposited on a glass substrate, with the sample solution placed directly on top of the metal film. Both configurations facilitate the detection of molecular binding events by monitoring changes in the SPR signal, which indicate alterations in the refractive index near the sensor surface (Zheng et al., 2020). One of the critical advantages of SPR sensors lies in their nanoscale sensitivity, allowing for the detection of minute changes in molecular interactions. Additionally, SPR sensors offer remote sensing capabilities, enabling real-time monitoring of biological processes without the need for labelling or extensive sample preparation. Furthermore, the high resolution of SPR sensors makes them particularly suitable for applications requiring precise and accurate measurements (Patel et al., 2020). SPR technology has been widely used in various fields, including clinical diagnostics, environmental monitoring, and biochemical analysis. SPR sensors can detect biomarkers indicative of disease states or monitor real-time drug interactions in clinical settings. Similarly, SPR sensors can detect pollutants or monitor water quality with high sensitivity and specificity in environmental applications. Beyond biomedical and environmental applications, SPR technology has also been applied in electronic systems, where it can be integrated into microfluidic platforms for lab-on-a-chip devices, as well as in studies of optical properties, such as plasmonic enhancement and surface-enhanced Raman spectroscopy (SERS) (Luan et al., 2018). Overall, SPR sensors represent a powerful tool for many applications, offering high sensitivity, resolution, and versatility in detecting molecular interactions. Their continued development and integration into various technologies promise further advancements in sensing and analytical capabilities.

Surface Plasmon Resonance (SPR) biosensors have become a powerful tool for detecting biological molecules. However, traditional approaches often rely on expensive and complex fabrication techniques. This section explores the growing interest in 2D nanomaterials like grapheme (Sbeah et al., 2022), black phosphorus, and chalcogenides (including GST) (Sbeah et al., 2022) for their potential to revolutionise SPR sensors. The unique electrical and optical properties of 2D nanomaterials hold immense promise for SPR sensor development (Helny et al., 2020). By precisely controlling the number of layers in these materials, researchers can tailor their electrical characteristics for enhanced biosensing capabilities. It translates to improved detection sensitivity for a wider range of biological molecules. Chemical Vapor Deposition (CVD) (Sbeah et al., 2023) has been the primary method for creating 2D nanomaterials for SPR sensors. However, this technique suffers from high costs and limitations in achieving desired results (Ji et al., 2021). Recent studies have explored innovative alternatives like electrospinning for producing 2D inorganic materials. This method offers advantages like continuous production, lower costs, and

improved safety. Modern SPR sensor designs often involve stacking multiple layers of 2D nanomaterials on a metal base. Researchers are actively exploring the development of heterostructures combining various 2D materials on a single chip (Xia et al., 2019). This approach aims further to enhance the performance and capabilities of SPR sensors. Over the past decade, researchers have focused on incorporating silicon (Si) into SPR sensors based on 2D nanomaterials. Studies have shown that increasing the number of graphene and silicon layers in such structures improves biomolecule adsorption, leading to better detection sensitivity (Verma et al., 2011; Ouyang, et al., 2016).

Recent research suggests that combining Si with GST on top of a metal layer can further enhance SPR sensor sensitivity. GST finds diverse applications ranging from refractive index-sensitive sensors to anti-radar detectors and tunable absorbers for aircraft invisibility technology applications (Patel et al., 2021). Moreover, GST plays a crucial role in enhancing the performance of plasmonic devices (Abdollahramezani et al., 2020). Its unique property of altering phase from amorphous (aGST) to crystalline (cGST) upon interaction with light makes it a versatile phase-change material for optical devices (Nejat and Nozhat, 2020). Furthermore, using phase change materials (PCMs), including GST, in biosensors facilitates the exploration of optimal resonances (Yan et al., 2019). In the context of surface plasmon resonance (SPR) based sensors, incorporating gold resonators with GST enhances tunability and improves sensitivity. This integration extends to applications like optical switches and modulators (Patel et al., 2020). MXenes, a recently discovered class of 2D transition metal carbides, nitrides, and carbonitrides (Kumar et al., 2022), are attracting significant attention due to their unique properties and vast application potential (Zhan et al., 2020). Their intense light absorption in the near-infrared region makes them promising candidates for SPR sensors (Lim et al., 2022). Among MXenes, Ti3C2Tx is a promising 2D material for biomolecule detection in SPR sensors (Sinha et al., 2018). Its exceptional properties, such as high mechanical and chemical stability, large surface area, and tunable plasmonic behaviour, make it a strong contender. However, achieving optimal performance requires precise control over its surface termination (Bai et al., 2016). Ti3C2Tx has the potential to be used in surface plasmon resonance (SPR) sensors for biomolecules; however, this use needs exact control of the material's surface termination. This study presents a numerical investigation of an SPR sensor design using GST, MXene, Silica, and Silver. We analyse the reflectance behaviour of this multi-layered structure across the infrared and visible wavelength spectrum to understand its suitability for various biosensing applications. By incorporating a diverse range of refractive indices in our simulations, we aim to assess the sensor's effectiveness for detecting a broad spectrum of biomolecules.

MODELLING AND THOERY

A refractive index sensor with a multi-layered structure has been presented in Figure 1 The proposed structure has been formed with Si-GST-Metal-MXene-Ag layers. The refractive index range is between 1 and 1.14, considered from the various material databases. That is why we consider the design to be a general refractive index sensor in the mentioned range. The middle metal layer is considered Ag/Au/Al/Cu to identify the effect of the metal layer on overall absorption and reflectance. The GST layer is configured as a state material aGST and cGST, where the different properties of the states are considered for identification of the tunable behaviour of the structure. The refractive indices range of GST changes with the change of temperature, and it has been taken from the graph given in [43], and it is in eV v/s permittivity that we have converted eV to wavelength range. The design is 2D and has been simulated using the finite element method (FEM) with the help of COMSOL Multiphysics software. In this design, a rectangular port

condition is used, and an infrared light wavelength of the range 0.7 to 2.5 μm is incident from the top of the structure from the first port, a y-polarized wave has been applied, and the second port is used for calculating the transmittance of the wave. The thickness of all material is chosen as 80 nm. The width of the GST and metal is considered as (W) 300 nm. The unit cell structure length is considered as (L) 300 nm.

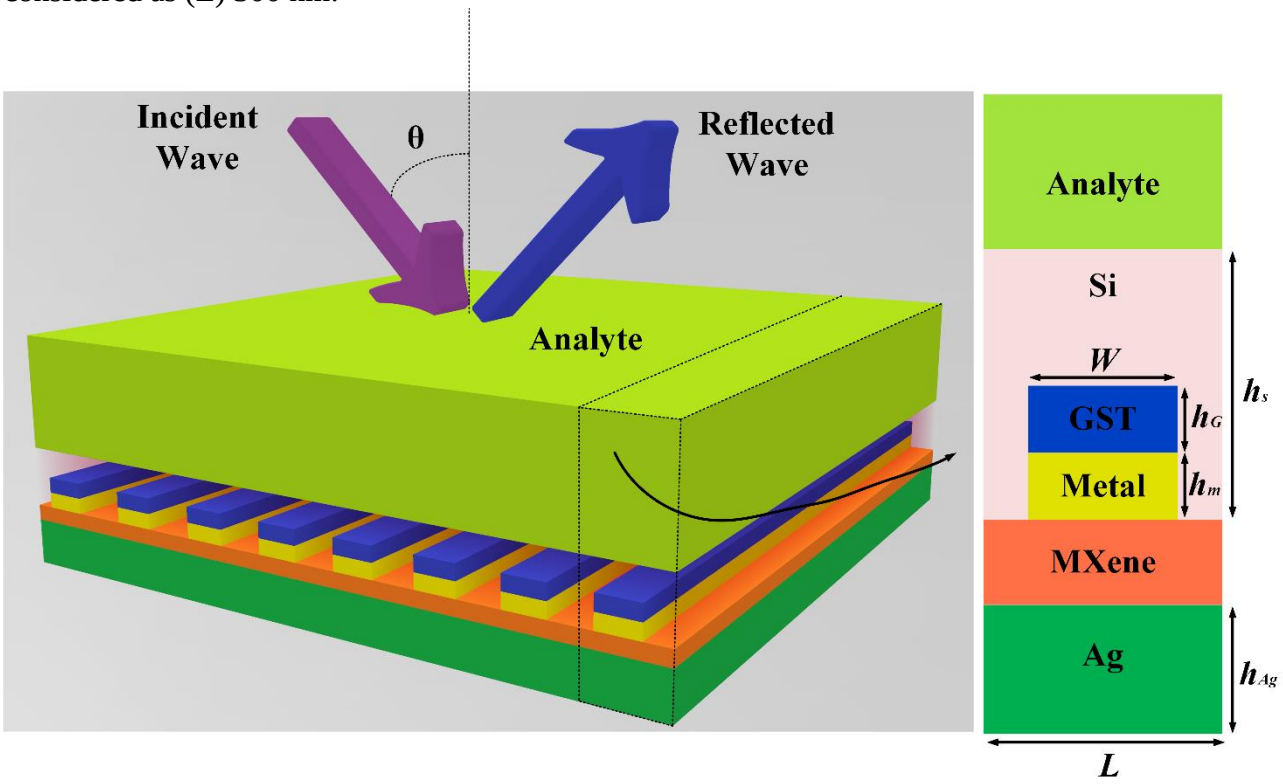

Figure 1: Schematic of the refractive index sensor with the multi-layered structure formed with Si-GST-Metal-MXene-Ag layers. (a) Schematic view of the proposed structure with the possible extended geometries projected for three-dimensional studies. (b) Two-dimensional front view of the structure used for the computational verification for the FEM studies. The various material databases consider the physical properties, such as refractive index/permittivity. The middle metal layer is considered Ag/Au/Al/Cu to identify the effect of the metal layer on overall absorption and reflector. The GST layer is configured as a state material aGST and cGST, where the different properties of the states are considered for identification of the tunable behaviour of the structure.

RESULTS AND DISCUSSION

The light transmitting in the multi-layered structure can be analysed using the Transfer Matrix Method for several layers. This method analyses how light propagates through layered materials, which is particularly useful when multiple interfaces exist (Troparevsky et al., 2010). The proposed design propagates in the Y direction, and for the one-dimensional cases, we have the energy equals:

$$E = \frac{\hbar^2}{2m}\left[k_{\parallel}^2 + k_{\perp}^2\right] \quad (1)$$

When we use the one-dimension propagation light, the $k_{\perp} \equiv 0$ and $k = \sqrt{k_{\parallel}^2 + k_{\perp}^2} = k$, then.

$$E = \frac{\hbar^2}{2m} k_{\parallel}^2 \quad (2)$$

The electromagnetic components of y-polarized incident light can be represented as follows:

$$\vec{E}_i = (E_x, 0, E_z) e^{j(k_x x + k_z - \omega t)} \left[\frac{V}{m}\right] \quad (2)$$

$$\vec{H}_i = (0, E_y, 0) e^{j(k_x x + k_z - \omega t)} \left[\frac{A}{m}\right] \quad (3)$$

By implementing the Maxwell equations with the proper boundary conditions, the resonance equation can be obtained in the following equation:

$$\frac{2\pi}{\lambda} \sqrt{\varepsilon_p} \sin\theta = \frac{\omega}{c} \sqrt{\frac{\varepsilon_m \varepsilon_a}{\varepsilon_m + \varepsilon_a}} \quad (4)$$

Where λ is the wavelength, ε_p is the permittivity of the prism, θ is the light incident angle, ω is the frequency, c the velocity of light, $\varepsilon_m \varepsilon_a$ are the permittivity for the metal and the surrounding medium, respectively. The previous equation can be rewritten as $k_y = \frac{2\pi}{\lambda_0} n_p \sin\theta = Re\{k_{sp}\}$. Where, k_y is the wave vector in the y direction, n_p is the refractive index of the prism, λ_0 is the wavelength in a vacuum, and $Re\{k_{sp}\}$ it is the real component of the SP wave vector in the y direction at the metal-dielectric interface.

While Fresnel equations accurately predict light reflection and transmission at a single interface, but with multiple layers, light undergoes partial reflection and continues propagating as waves at each interface. The Transfer-Matrix Method (TMM) provides a powerful alternative, employing specific equations to describe this complex light propagation through layered materials, as we can see in the following equation:

$$t = 2ik_L e^{-ik_R L} \left[\frac{1}{-M_{21} + k_R k_L M_{12} + i(k_R M_{11} + k_L M_{22})}\right] \quad (5)$$

and

$$r = \left[\frac{(M_{21} + k_R k_L M_{12}) + i(k_L M_{22} - k_R M_{11})}{(-M_{21} + k_R k_L M_{12}) + i(k_R M_{11} + k_L M_{22})}\right] \quad (6)$$

Where k_R is the wavenumber in the rightmost medium, and $k_L$is the wavenumber in the left medium M_{mn} is the matrix elements. The reflectance and transmittance are given by $T = \frac{k_R}{k_L}|t|^2$ and $R = |r|^2$ respectively. The phase sensitivity detection can determine the sensitivity of the proposed design, and it can be expressed as:

$$S = \frac{\Delta\theta}{\Delta n} \quad (7)$$

The refractive index of the silicon has been reported in (Aliqab, 2023). The refractive indices of aGST and cGST were determined using a frequency field between 100 THz to 800 THz. The aGST real part is in the range of 2.6 to 4.6, the imaginary part is from 0 to 2.4, the real part of cGST is in the range of 2.25 to 7.16, and the imaginary part is from 0 to 4.1 (Shpaortko et al., 2008). The optical properties of gold have been taken from the table reported in (Johnson et al., 1972).

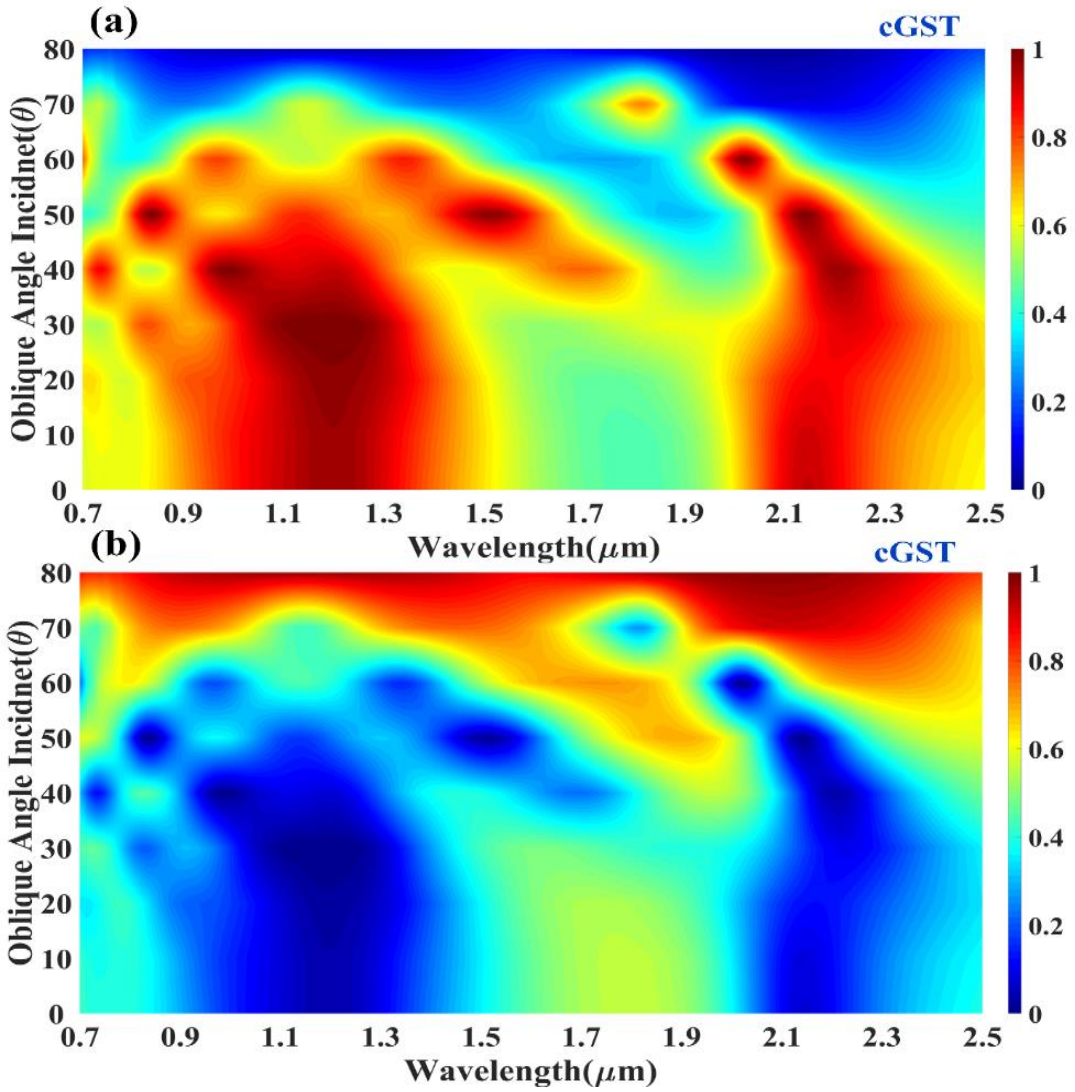

Figure 2: Calculated variation in the (a) absorption and (b) reflectance for the different values of the oblique angle incident and wavelength. The results of the cGST phase of the GST material have been calculated. The metal layer is considered as Au for the simulations.

Absorption and Reflectance for GST Based on Au

We observe the absorption and reflectance responses in **Error! Reference source not found.** and Figure 2. The reflectance and transmittance can be calculated using the TMM to study the performance properties of the proposed structure, as mentioned in equations 5 and 6. Absorption can be calculated using the equation:

$$A = 1 - T + R \quad (9)$$

We investigated the absorbance spectrum for the proposed design using COMSOL Multiphysics software. Figure 2(a) shows the absorption and reflectance responses for the aGST phase of the GST material. The absorption and reflectance changes with different oblique incident angles. The simulations considered a gold (Au) metal layer and varied the angle of incidence from 0° to 80° in 10° steps. The results showed an absorption sensitivity to both the incident angle and wavelength. This is because the structure creates multiple resonance conditions across the wavelength spectrum.

Interestingly, absorption increases with a lower oblique incident angle and at two different wavelength bands. Additionally, the polarisation angle of the incident light affects the overall behaviour of the structure. Similarly, Figure 2 shows the absorption and reflectance responses for the cGST phase of the GST material. The resonance values of the individual peak are sensitive to the phase of the GST material. We can observe that the peak values are shifted to different wavelength ranges for the cGST phase compared to the aGST phase, which has higher absorbance.

Effect of Oblique Angle Incident

Understanding how oblique angle incidence affects a refractive index sensor is essential in photonics and optical engineering for various reasons. Refractive index sensors are utilized to quantify the refractive index of materials, a key optical property that indicates how light travels through a substance. These sensors are widely used in environmental monitoring, biomedical diagnostics, chemical analysis, and various other fields. Comprehending the impact of oblique angle incidence on these sensors can greatly improve their performance and expand their range of applications. Oblique angle incidence can impact the sensitivity and selectivity of refractive index sensors. When light enters a medium at an angle, the distance it travels through the sensing region increases, potentially improving the sensor's ability to interact with the substance being analyzed. This can result in increased sensitivity as the alteration in the refractive index caused by a particular analyte becomes more noticeable. Adjusting the angle of incidence can optimize the sensor for particular applications, improving its ability to detect specific compounds or conditions. Identifying oblique angle effects is crucial for accurately modeling and designing refractive index sensors. Optical simulations and designs typically assume light enters at normal incidence, but in real-world scenarios, light can come in at different angles. Comprehending these impacts enables the creation of more precise models, resulting in the development of sensors with enhanced performance. Moreover, the impact of oblique angle incidence can affect the production and incorporation of refractive index sensors into larger systems. In systems with limited space or specific geometrical requirements, sensors need to function effectively at non-normal angles. Understanding the impact of oblique angles on sensor performance is crucial for incorporating these devices into intricate optical systems or compact instruments. Studying oblique angle incidence on refractive index sensors is crucial for improving their sensitivity and selectivity, enhancing modeling and design accuracy, and aiding in their integration into larger systems. This knowledge advances optical sensor technology and broadens their practical applications in scientific and industrial sectors.The magnetic field enhancement at the important interfacing points of the proposed design.

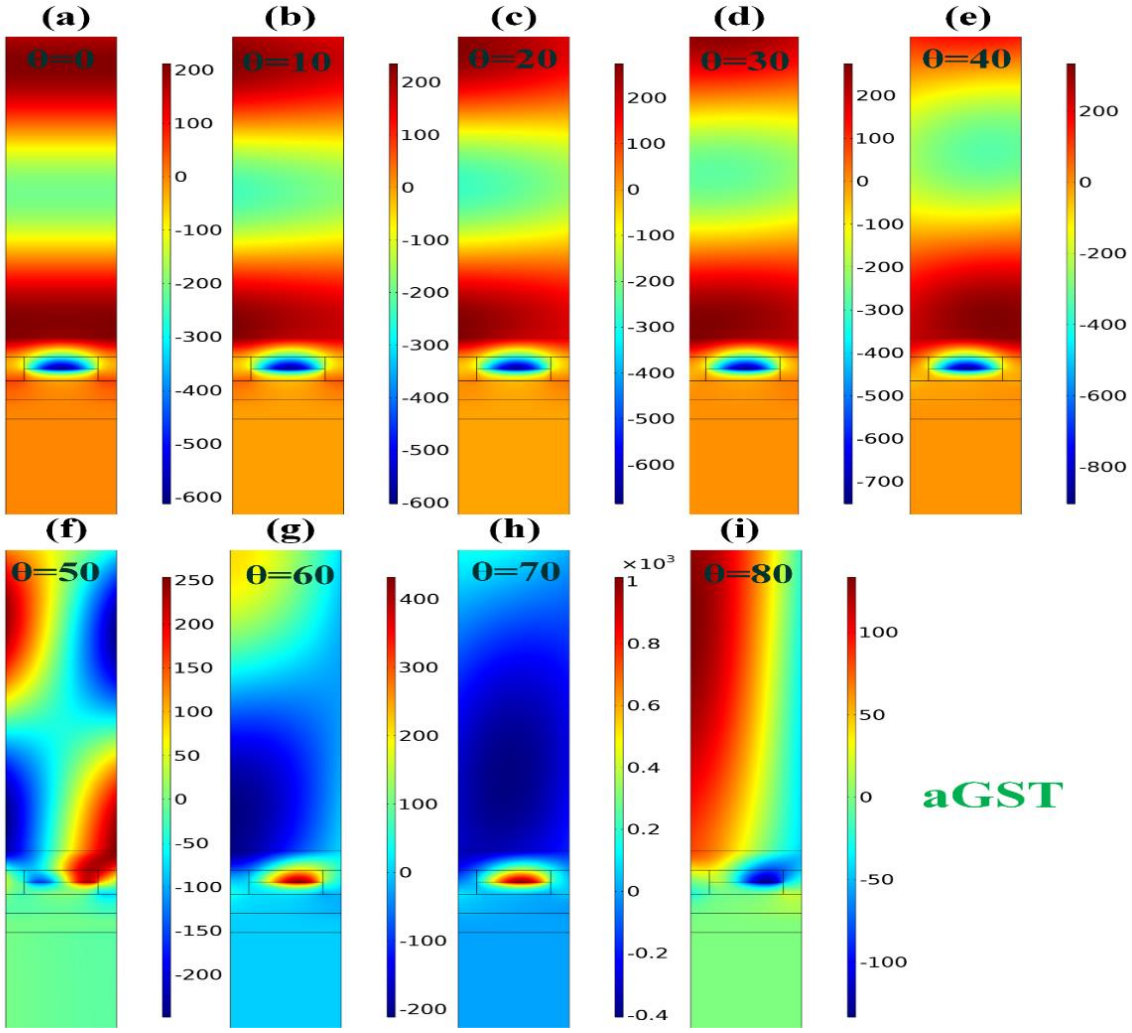

Figure 3: Magnetic field distribution over the entire structure for different incident angles varies from (a-i) 0^o - 80^o for the a-GST phase.

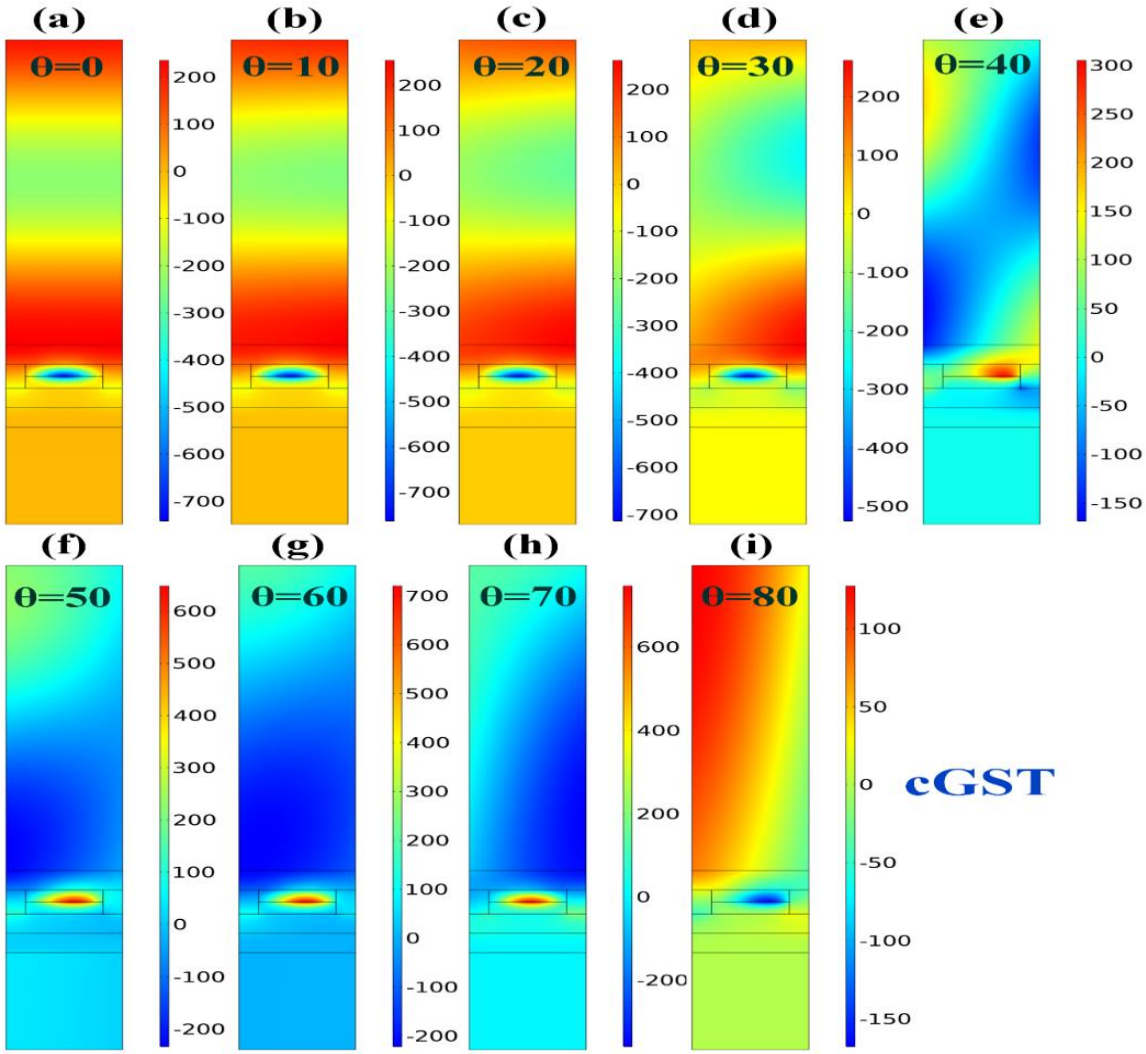

Figure 4: Magnetic field distribution over the entire structure for different incident angles varies from (a-i) 0^o - 80^o for the c-GST phase.

The sensitivity of sensors depends on the transverse magnetic field in the different interfaces of the structure. To analyse the excitation and field distribution, we investigated the Magnetic field distribution over the entire structure for various angles of incident of the proposed design using COMSOL Multiphysics software. The magnetic field distribution varies with the change of oblique angle incident from 0° to 80° in 10° steps for the aGST phase, as shown in Figure 3. The effect of the oblique angle incident on the proposed structure's overall performance shows that the field intensity values are higher at the transverse points of the structure. Similarly, Figure 4 shows the variation of magnetic field intensity with the change of oblique angle incident from 0° to 80° in 10° steps for the cGST phase. The field intensity values are higher at the lower angles at the transverse points of the structure in both phases. Based on previously published literature, the refractive indices of various materials such as water, ethanol, blood plasma, urine, glucose, and haemoglobin range from 1 to 2.5. μm Resonant wavelengths, corresponding to peaks in transmittance, play a crucial role in sensing applications. Fundamentally, for a refractive index (RI) sensor, any change in the refractive index will result in a shift in the angle of the resonant wavelength in the wavelength

regions. These shifts, known as resonance peaks, enable the identification of unknown materials. In the context of sensing, detecting an unknown analyte through SPR biosensors can be achieved by monitoring changes in the wavelength of reflected light and observing changes in the angle of incidence. These different approaches to sensing show us the importance of understanding how variations in refractive index and other parameters influence resonance phenomena, offering valuable insights into developing robust sensing technologies for diverse applications.

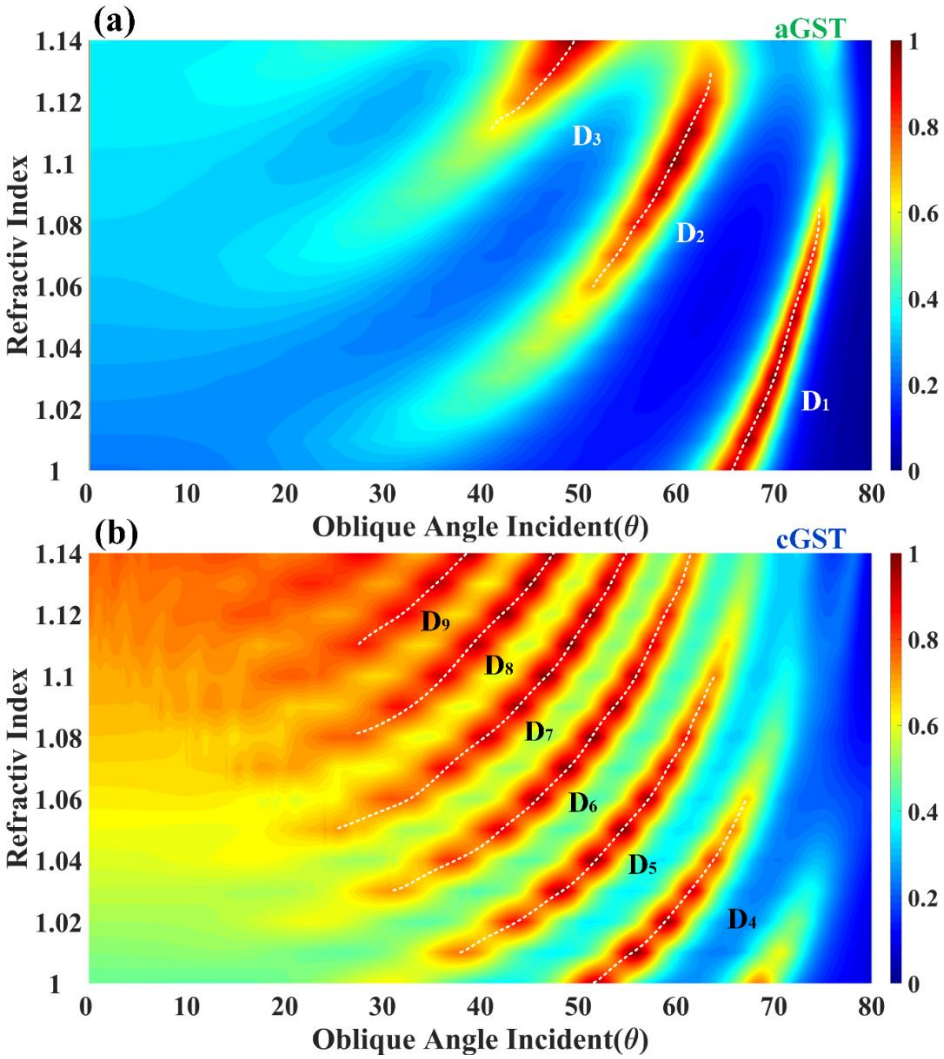

Figure 5: Calculated absorption peaks for the different values of the refractive index and oblique angle incident for (a) aGST and (b) cGST of the phases of the GST material.

Sensitivity of GST For Different Values of Refractive Index and Oblique Incident

SPR sensors work by utilising impedance matching to identify alterations in a materials index. These sensors use the interaction between surface plasmons, which are electron oscillations at the boundary between a metal film and a dielectric substance. When light hits the sensor at an angle, it can transfer its energy to the surface plasmons, resulting in a state. This resonance appears as a drop in the reflected light spectrum called the peak. The position of this peak on the wavelength spectrum is susceptible to changes in the index of the material to the metal film. As the index of the detected material shifts, adjustments in how light and surface plasmons interact happen, leading to movement of the peak on the wavelength spectrum. By tracking this movement, SPR sensors can detect fluctuations in the index of their environment, making them valuable tools for various sensing tasks.

The formula for calculating sensor sensitivity based on the oblique incident angle is mentioned in Equation 7. Where $\Delta\theta$ is the difference between the angles of the absorption response peaks, and Δn is the difference between the refractive indices at those peaks. Sensitivity will be affected by the change in refractive index that occurs when GST is at the aGST phase or the cGST phase. From Figure 5, These absorption values are considered for the 1.5 μm of the constant wavelength while simulating the aGST and cGST phases of the overall structure. we can notice that aGST on the same wavelength provided is showing three significant responses at the higher oblique incident angles from 40° to 80°. On the other hand, cGST is showing six primary traces for the same wavelength of simulation, with a higher density response all over the full range of the incident light angles with lesser density at the 70° and 80°. SPRs are used to implement the theory of match impedance due to the detected material's shifting in the refractive index. The resonant peaks of the absorption spectrum shift when the sensed material refractive indices change because of this change in refractive index. Table 1 shows the derived equations of the quadric regression for the refractive index's sensitivity per incident angle of the two phases, aGST and cGST, for the proposed design. This formula can be a foundation for creating a biosensor to identify substances with refractive indices, each displaying unique resonance peaks at specific wavelengths. The refractive index of these molecules typically ranges from 1 to 1.4. Varies based on the concentration of the biomarker. This study shows the important role of metamaterial plasmonic sensors in elevating the sensing parameters such as sensitivity (S), figure of merit (FoM), and quality factor (Q-factor). Leveraging active materials and their inherent properties further enhances these parameters, particularly in sensing applications. Metamaterials offer significant advantages in the fabrication and simulation of sensors and absorbers, presenting a more straightforward design process than other topologies. The advantage of using metamaterials is their ability to enhance the number of reflected waves within the structure, amplifying sensitivity and enhancing light absorption characteristics. The resonance peak angles undergo shifts influenced by factors such as the active material's absorption of light within the operated wavelength range and changes in the material's refractive index during sensing. In another way, metamaterial plasmonic sensors not only optimise key parameters of the design but also provide a flexible platform for advancing sensing technologies through the strategic integration of active materials and precise control over resonance phenomena.

Table 1: Derived equations for the refractive index's sensitivity per incident angle of the two phases a-GST and c-GST for the proposed design

Phase	Traces	RI	Angle	Quadratic regression	Maximum (deg/RIU)	Minimum (deg/RIU
aGST	D_1	1 – 1.07	65.70°– 73.80°	$\theta = -581.4842\, n^2 + 1318.21n - 670.97$	159	80
	D_2	1.08 – 1.12	55.99°– 62.60°	$\theta = -1143.46\, n^2 + 2679.67n - 1504.28$	209	130
	D_3	1.13 – 1.15	46.99°– 51.00°	$\theta = -1999.62n^2 + 4759.16n - 2777.53$	220	180
cGST	D_4	1 – 1.04	51.79°– 63.79°	$\theta = -3144.31n^2 + 6712.36n - 3516.22$	399	220
	D_5	1.02 – 1.08	43.70°– 61.00°	$\theta = -2498.23n^2 + 5530.59n - 2998.21$	439	180
	D_6	1.04 – 1.12	37.10°– 59.10°	$\theta = -2106.94n^2 + 4817.16n - 2693.43$	360	150
	D_7	1.07 – 1.15	36.50°– 56.40°	$\theta = -1691.35n^2 + 3997.96n - 2304.63$	409	150
	D_8	1.09 – 1.14	31.79°– 49.39°	$\theta = -5571.50n^2 + 12750.17n - 7245.58$	770	209
	D_9	1.11- 1.15	27.78°– 41.40°	$\theta = -2498.09n^2 + 5985.14n - 3537.79$	418	270

Optimisation and Validation

This study explores how optimising device parameters can significantly improve the sensor's sensitivity for detecting refractive index changes in materials. Parameters like the width and height of different layers are crucial in achieving this goal. By carefully tailoring these dimensions, we observe a distinct shift in the absorption response between the amorphous (aGST) and crystalline (cGST) phases of the GST material. This shift is instrumental in precisely identifying the refractive index of the sensed material. From Figure 6, we can observe the effect of changing the height of the metal layer (h_m). The variation in the absorption responses for the change in the height of the metal layer shows that the absorption values are not linearly changing with the wavelength in aGST phase. However, the cGST phase changes linearly with the wavelength over the full range of the wavelength spectrum. We can observe a shift between the two phases. The change in the multi-layered middle resonator (W) (metal-GST) for absorption variation for different phases aGST and cGST of the phase change material has been shown in Figure 7. The absorption values are linearly changing with the wavelength in aGST phase over 0.9 to 1.7μm of the wavelength. The exact linear change for the same spectrum is not observed in the cGST phase. From the Figure 8, we calculated the absorption variations for the different values of the Si height for the different phases of the GST material aGST and cGST. The values of the h_{Si} is highly sensitive for the effective resonance of the material. The values of the absorption peak are linearly varied for the different height values over the wavelength spectrum for both GST phases. The effect of changing the bottom metal layered height (h_{Ag}) for the absorption spectrum has been shown in Figure 9. The values of the absorption are constant for the any values of the Ag material height over the entire spectrum. Figure 11 shows

the variations in the absorption responses for the different metals chosen to fort the middle resonator. Absorption is calculated for Ag/Au/Cu/Al materials. The reaction of the aGST and cGST phases of the phase change material has also been investigated. It can be noticed that the metal Au is showing a shift in the wavelength spectrum compared to the other metals.

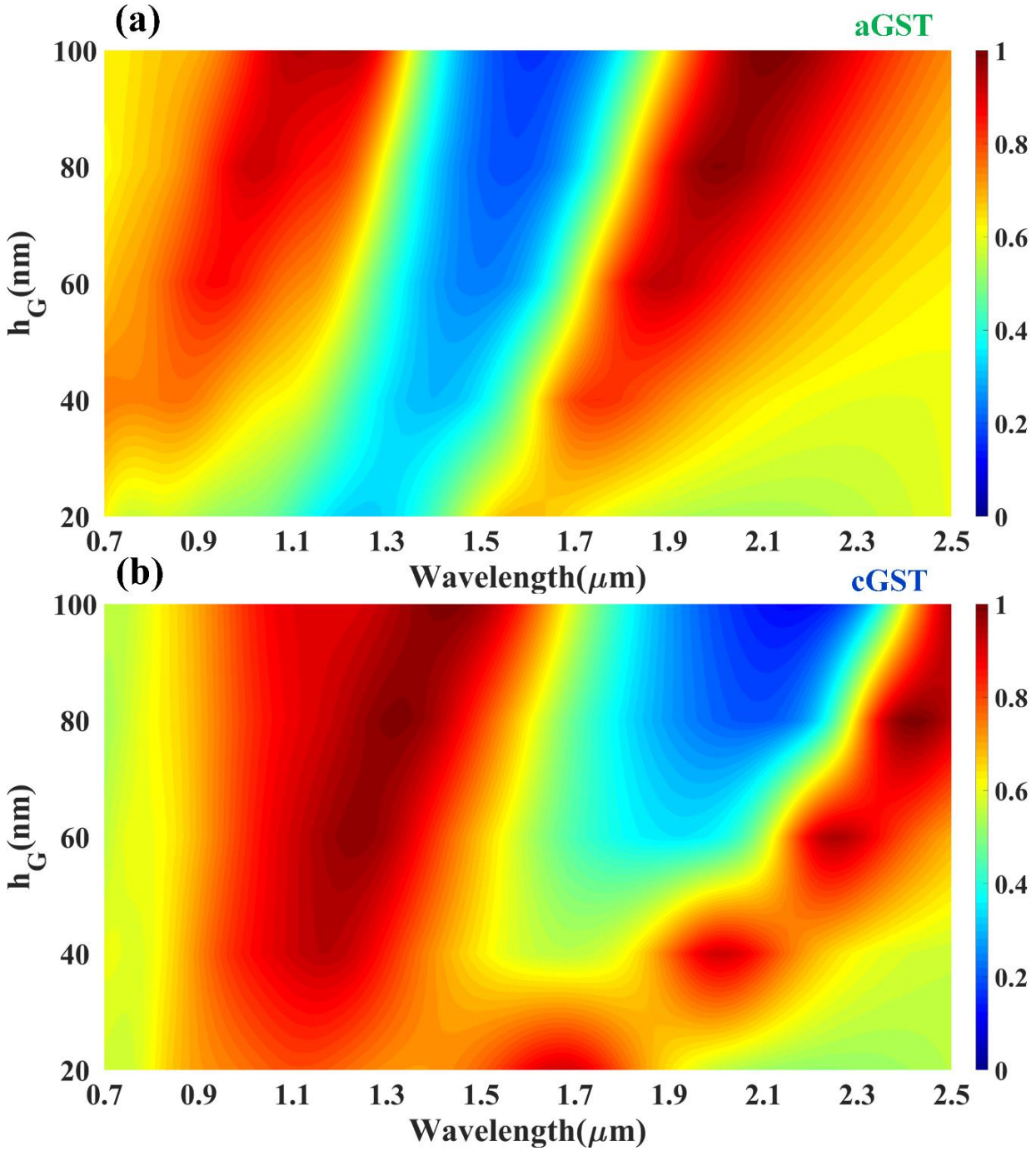

Figure 6: Variation in the absorption for the different heights of the metal layer h_m. The absorption effect is calculated for the height values of 20-100 nm for (a) aGST and (b) cGST phase of the GST material.

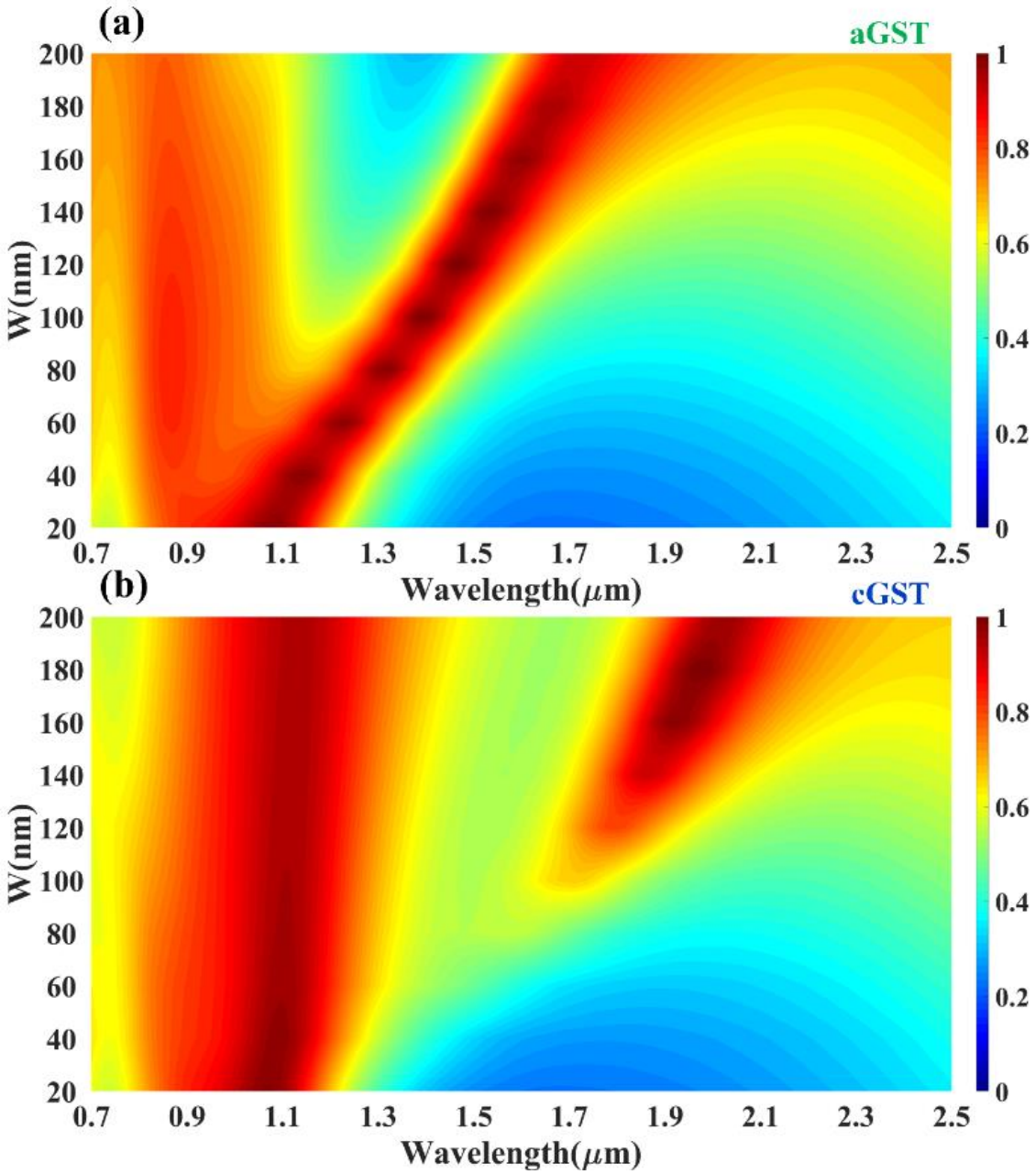

Figure 7: Effect of the change in the multi-layered middle resonator (W) (metal-GST) for absorption variation for different (a) aGST and (b) cGST of the phase change material.

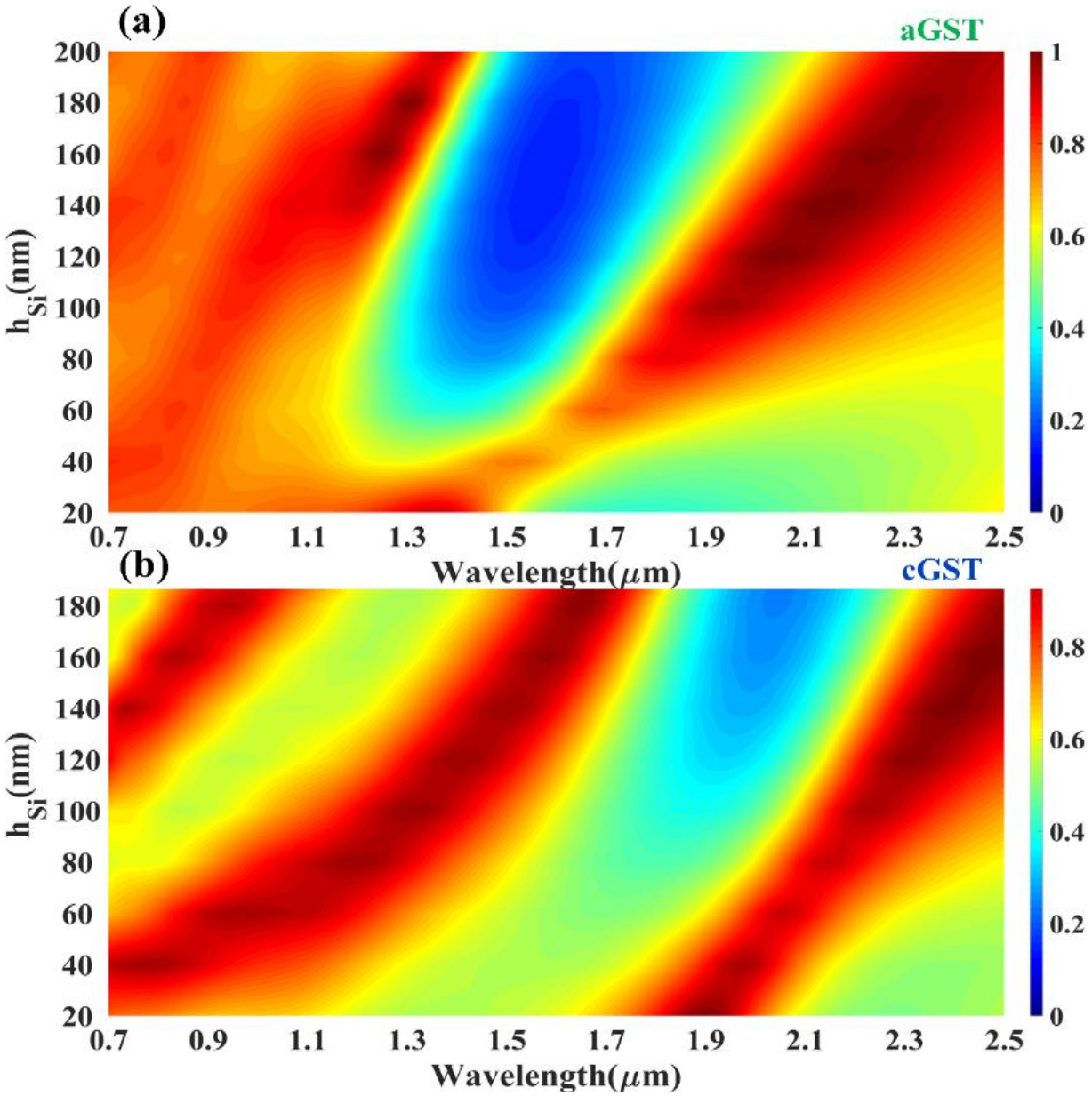

Figure 8: Calculated absorption variation for the different values of the Si height for the different phases of the GST material.

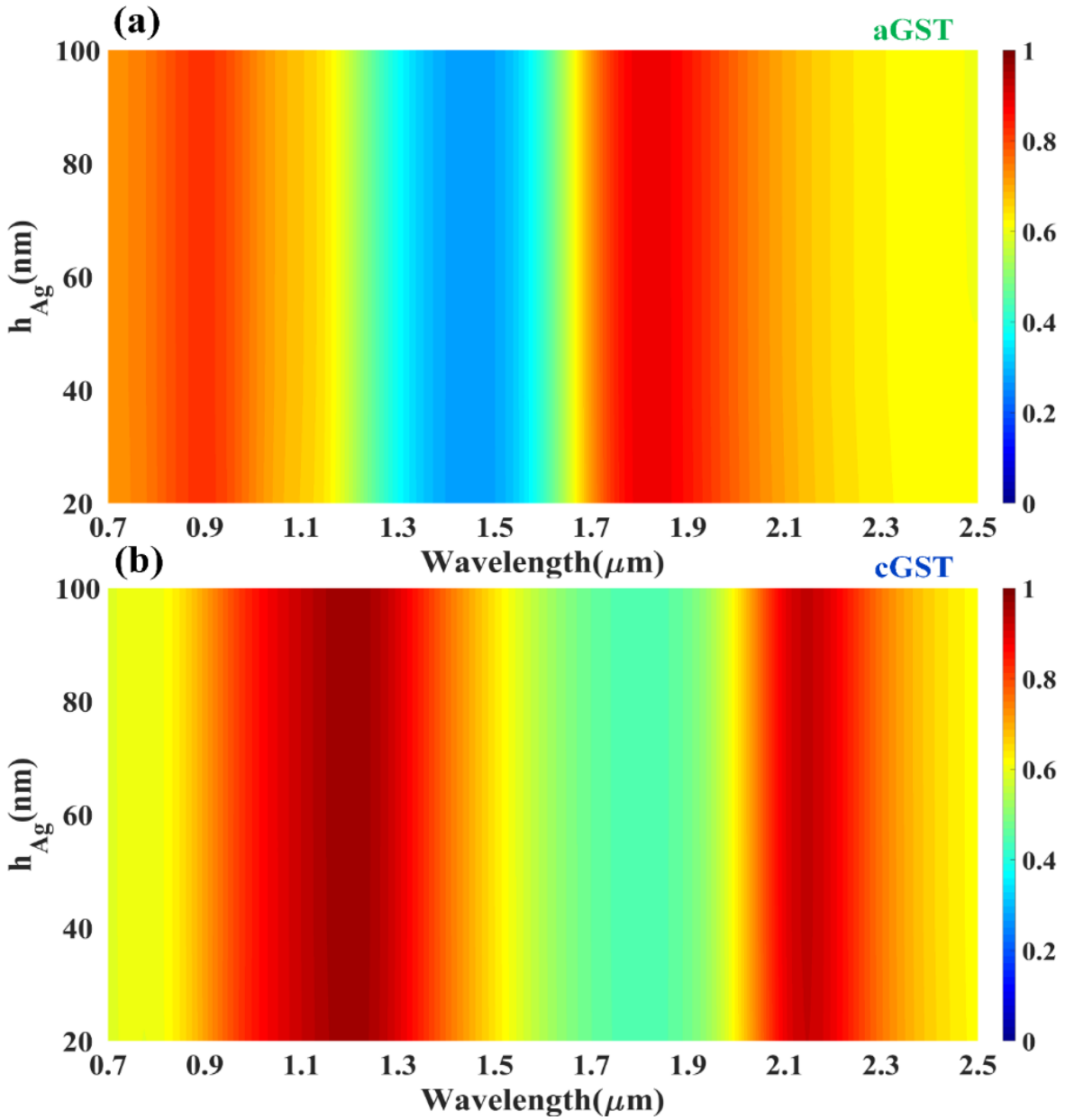

Figure 9: Effect of the bottom metal layered height ($\boldsymbol{h_{Ag}}$) for the absorption spectrum.

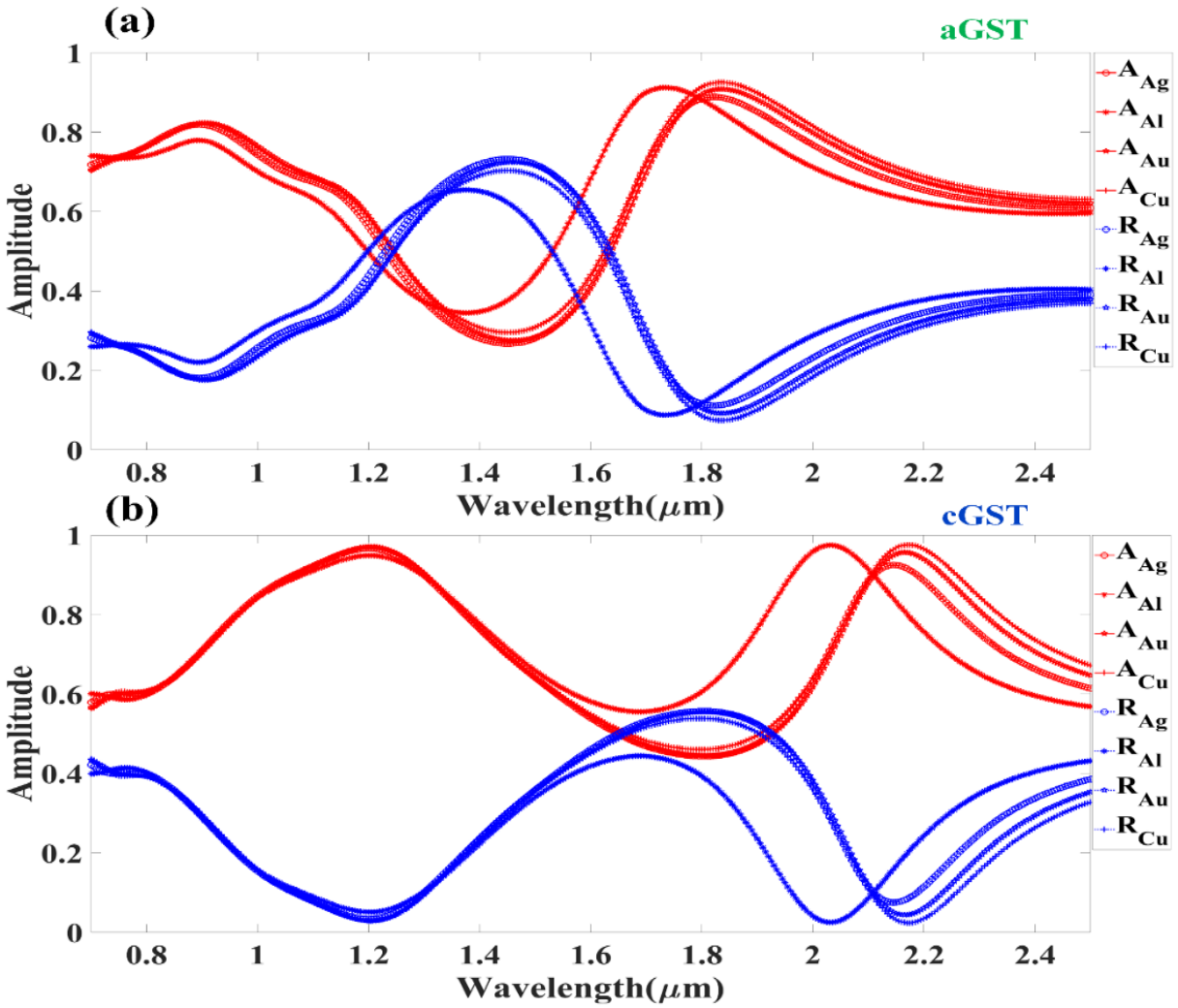

Figure. 10. Variation in the absorption for the different metals chosen to fort the middle resonator. Absorption is calculated for Ag/Au/Cu/Al materials. The response for (a) aGST and (b) cGST phases of the phase change material has also been investigated.

CONCLUSIONS

This paper proposes a general RF sensor design for material detection utilising GST (gratings with a phase change material) and MXene as active components. This refractive index sensor can work for a wide infrared and visible frequency range of 0.7 µm to 2.5 µm. The sensor exhibits tunability varying sensitivity depending on the GST phase (amorphous or crystalline). The study investigated the influence of oblique incident light angles on absorption at different wavelengths. We presented both phases' absorption and reflectance responses based on the gold (Au) layer. Furthermore, the magnetic field distribution across the entire structure was analysed for various incident angles (0° to 80°) for both aGST and cGST phases. We derived equations to calculate the refractive index sensitivity per incident angle for each phase within the proposed design. Additionally, optimisation and validation for different parameters like height and width and different metals were conducted for Ag/Au/Cu/Al processes to ensure optimal device performance. Overall bandwidth and the resonating region are different for both phases. This sensor can offer the minimum and maximum

sensitivity of 80 deg/RIU and 770 deg/RIU, respectively. The proposed design has potential applications in detecting different refractive index molecules with refractive index varying between 1 and 1.14.

REFERENCES

Abdollahramezani, S., Hemmatyar, O., Taghinejad, H., et al. (2020). Tunable nanophotonics enabled by chalcogenide phase-change materials. *Nanophotonics, 9*(5), 1189–1241. https://doi.org/10.1515/nanoph-2020-0039/xml

Adhikari, R., Sbeah, Z. A., Chauhan, D., et al. (2022). Enhanced coupling efficiency in metal–dielectric–metal waveguide-ring structure for plasmonic temperature sensor and sucrose concentration detector. *Optik, 264*, 169425. https://doi.org/10.1016/j.ijleo.2022.169425

Aieta, F., Genevet, P., Khorasaninejad, M., Yu, N., Kats, M. A., Gaburro, Z., & Capasso, F. (2017). Recent advances in planar optics: From plasmonic to dielectric metasurfaces. *Optica, 4*(1), 139–152. https://doi.org/10.1364/OPTICA.4.000139

Aliqab, K., Sorathiya, V., Alsharari, M., et al. (2023). Numerical analysis of hafnium oxide and phase change material-based multi-layered infrared and visible frequency sensor for biomolecules sensing application. *Scientific Reports, 13*(1), 1–19. https://doi.org/10.1038/s41598-023-34817-1

Atabaki, A. H., Moazeni, S., Pavanello, F., et al. (2018). Integrating photonics with silicon nanoelectronics for the next generation of systems on a chip. *Nature, 556*(7701), 349–354. https://doi.org/10.1038/s41586-018-0028-z

Bai, Y., Zhou, K., Srikanth, N., et al. (2016). Dependence of elastic and optical properties on surface terminated groups in two-dimensional MXene monolayers: A first-principles study. *RSC Advances, 6*(43), 35731–35739. https://doi.org/10.1039/c6ra03090d

Caloz, C., & Itoh, T. (2005). Fundamentals of LH MTMs. In *Electromagnetic Metamaterials: Transmission Line Theory and Microwave Applications* (pp. 27–58). Wiley. https://doi.org/10.1002/0471754323.CH2

Chauhan, D., Kumar, A., Adhikari, R., & Shukla, A. (2021). High performance vanadium dioxide-based active nano plasmonic filter and switch. *Optik, 225*, Article 165672. https://doi.org/10.1016/j.ijleo.2020.165672

Dickson, W., Wurtz, G. A., Evans, P. R., et al. (2008). Electronically controlled surface plasmon dispersion and optical transmission through metallic hole arrays using liquid crystal. *Nano Letters, 8*(1), 281–286. https://doi.org/10.1021/nl072613g

Helmy, A. S., Engheta, N., Lin, C., & Chang, P.-H. (2020). Tailoring of modal losses in anisotropic 2D material ribbons by regulating material absorption. *Journal of the Optical Society of America B, 37*(12), 3681–3689. https://doi.org/10.1364/josab.403100

Ji, W., Zhao, G., Guo, C., et al. (2021). A novel method to fabricate two-dimensional nanomaterial based on electrospinning. *Composites Part A: Applied Science and Manufacturing, 143*, 106275. https://doi.org/10.1016/j.compositesa.2021.106275

Jiang, N., Zhuo, X., & Wang, J. (2018). Active plasmonics: Principles, structures, and applications. *Chemical Reviews, 118*(6), 3054–3099. https://doi.org/10.1021/acs.chemrev.7b00252

Jaggard, D. L., Mickelson, A. R., & Papas, C. H. (1979). On electromagnetic waves in chiral media. *Applied Physics, 18*(2), 211–216. https://doi.org/10.1007/BF00934418

Johnson, P. B., & Christy, R. W. (1972). Optical constants of the noble metals. *Physical Review B, 6*(12), 4370–4379. https://doi.org/10.1103/PhysRevB.6.4370

Kaushik, S., Tiwari, U. K., Deep, A., & Sinha, R. K. (2019). Two-dimensional transition metal dichalcogenides assisted biofunctionalized optical fiber SPR biosensor for efficient and rapid detection of bovine serum albumin. *Scientific Reports, 9*, Article 43531. https://doi.org/10.1038/s41598-019-43531-w

Khan, S., & Eibert, T. F. (2018). A multifunctional metamaterial-based dual-band isotropic frequency-selective surface. *IEEE Transactions on Antennas and Propagation, 66*(8), 4042–4051. https://doi.org/10.1109/TAP.2018.2835667

Kivshar, Y. S. (2009). Nonlinear and tunable metamaterials. In *Metamaterials: Fundamentals and Applications II* (Vol. 7392, p. 739217). SPIE. https://doi.org/10.1117/12.827872

Kumar, J. A., Prakash, P., Krithiga, T., et al. (2022). Methods of synthesis, characteristics, and environmental applications of MXene: A comprehensive review. *Chemosphere, 286*, 131607. https://doi.org/10.1016/j.chemosphere.2021.131607

Lerner, M. B., Matsunaga, F., Han, G. H., et al. (2014). Scalable production of highly sensitive nanosensors based on graphene functionalized with a designed G protein-coupled receptor. *Nano Letters*. https://doi.org/10.1021/nl5006349

Lim, K. R. G., Shekhirev, M., Wyatt, B. C., et al. (2022). Fundamentals of MXene synthesis. *Nature Synthesis, 1*(8), 601–614. https://doi.org/10.1038/s44160-022-00104-6

Luan, E., Shoman, H., Ratner, D. M., et al. (2018). Silicon photonic biosensors using label-free detection. *Sensors (Switzerland), 18*(10), 3519. https://doi.org/10.3390/s18103519

Nejat, M., & Nozhat, N. (2020). Sensing and switching capabilities of a tunable GST-based perfect absorber in the near-infrared region. *Journal of Physics D: Applied Physics, 53*(24), 245105. https://doi.org/10.1088/1361-6463/ab7d6a

Ouyang, Q., Zeng, S., Jiang, L., et al. (2016). Sensitivity enhancement of transition metal dichalcogenides/silicon nanostructure-based surface plasmon resonance biosensor. *Scientific Reports, 6*(1), 28190. https://doi.org/10.1038/srep28190

Patel, S. K., Parmar, J., Sorathiya, V., & Nguyen, T. K. (2021). Tunable infrared metamaterial based. [Details on page numbers or volume/issue should be added if available.]

Patel, S. K., Parmar, J., Trivedi, H., et al. (2020). Highly sensitive graphene-based refractive index biosensor using gold metasurface array. *IEEE Photonics Technology Letters, 32*(8), 681–684. https://doi.org/10.1109/lpt.2020.2992085

Patel, S. K., Parmar, J., Kosta, Y. P., et al. (2020). Graphene-based highly sensitive refractive index biosensors using C-shaped metasurface. *IEEE Sensors Journal, 20*(18), 10365–10372. https://doi.org/10.1109/jsen.2020.2976571

Rahmat-Samii, Y. (2006). Metamaterials in antenna applications: Classifications, designs, and applications. In *2006 IEEE International Workshop on Antenna Technology: Small Antennas and Novel Metamaterials* (pp. 1–4). IEEE. https://doi.org/10.1109/IWAT.2006.1608960

Rickman, A. (2014). The commercialisation of silicon photonics. *Nature Photonics, 8*(8), 579–582. https://doi.org/10.1038/nphoton.2014.175

RP Photonics Encyclopedia. (n.d.). Photonic metamaterials: Nanotechnology, negative-index media, negative refraction, cloaking. RP Photonics. Retrieved November 21, 2022, from https://www.rp-photonics.com/photonic_metamaterials.html

Sbeah, Z. A., Adhikari, R., Sorathiya, V., et al. (2023). High-sensitive plasmonic multilayer SiO2/VO2 metamaterial sensor. *Applied Physics A: Materials Science & Processing, 129*(1), 1–17. https://doi.org/10.1007/s00339-023-06846-0

Sbeah, Z. A., Adhikari, R., Sorathiya, V., et al. (2022). GST-based plasmonic biosensor for hemoglobin and urine detection. *Plasmonics, 17*(1), 1–14. https://doi.org/10.1007/s11468-022-01728-2

Sbeah, Z. A., Adhikari, R., Sorathiya, V., et al. (2023). A review on metamaterial sensors based on active plasmonic materials. *Plasmonics, 18*, 1–20. https://doi.org/10.1007/s11468-023-01904-y

Sbeah, Z. A., Dwivedi, R. P., Sorathiya, V., et al. (2022). Graphene assisted tunable narrowband metamaterial absorber for infrared wavelength. *AIP Conference Proceedings, 2640*(1), 020007. https://doi.org/10.1063/5.0110056

Sbeah, Z. A., Dwivedi, R. P., Sorathiya, V., et al. (2022). Phase change material-based biosensor in infrared frequency spectrum. *AIP Conference Proceedings, 2640*(1), 020008. https://doi.org/10.1063/5.0110060

Shportko, K., Kremers, S., Woda, M., et al. (2008). Resonant bonding in crystalline phase-change materials. *Nature Materials, 7*(8), 653–658. https://doi.org/10.1038/nmat2226

Sinha, A., Dhanjai, Zhao, H., et al. (2018). MXene: An emerging material for sensing and biosensing. *TrAC Trends in Analytical Chemistry, 105*, 424–435. https://doi.org/10.1016/j.trac.2018.05.021

Singh, G., Ni, R., & Marwaha, A. (2015). A review of metamaterials and its applications. *International Journal of Engineering Trends and Technology, 19*(4), 305–310. https://doi.org/10.14445/22315381/IJETT-V19P254

Stevenson, P. R., Du, M., Cherqui, C., et al. (2020). Active plasmonics and active chiral plasmonics through orientation-dependent multipolar interactions. *ACS Nano, 14*(11), 11518–11532. https://doi.org/10.1021/acsnano.0c03971

Sun, C., Wade, M. T., Lee, Y., et al. (2015). Single-chip microprocessor that communicates directly using light. *Nature, 528*(7583), 534–538. https://doi.org/10.1038/nature16454

Thomson, D., Zilkie, A., Bowers, J. E., Komljenovic, T., Reed, G. T., Vivien, L., Marris-Morini, D., Cassan, E., Virot, L., Fedeli, J. M., & Hartmann, J. M. (2016). Roadmap on silicon photonics. *Journal of Optics, 18*(7), Article 073003. https://doi.org/10.1088/2040-8978/18/7/073003

Tokarev, I., Tokareva, I., Gopishetty, V., et al. (2010). Specific biochemical-to-optical signal transduction by responsive thin hydrogel films loaded with noble metal nanoparticles. *Advanced Materials, 22*(12), 1412–1416. https://doi.org/10.1002/adma.200903456

Troparevsky, M. C., Lupini, A. R., Sabau, A. S., & Zhang, Z. (2010). Transfer-matrix formalism for the calculation of optical response in multilayer systems: From coherent to incoherent interference. *Optics Express, 18*(24), 24715–24721. https://doi.org/10.1364/oe.18.024715

Verma, R., Gupta, B. D., & Jha, R. (2011). Sensitivity enhancement of a surface plasmon resonance-based biomolecules sensor using graphene and silicon layers. *Sensors and Actuators B: Chemical, 160*(1), 623–631. https://doi.org/10.1016/j.snb.2011.08.039

Veselago, V. G. (1968). The electrodynamics of substances with simultaneously negative values of ε and μ. *Soviet Physics Uspekhi, 10*(4), 509-514. https://doi.org/10.1070/PU1968V010N04ABEH003699

Xia, G., Zhou, C., Jin, S., et al. (2019). Sensitivity enhancement of two-dimensional materials based on genetic optimisation in surface plasmon resonance. *Sensors, 19*(5), 1198. https://doi.org/10.3390/s19051198

Yan, X., Yang, M., Zhang, Z., et al. (2019). The terahertz electromagnetically induced transparency-like metamaterials for sensitive biosensors in the detection of cancer cells. *Biosensors and Bioelectronics, 126*, 485–492. https://doi.org/10.1016/j.bios.2018.11.014

Zeng, W., Shu, L., Li, Q., et al. (2014). Fiber-based wearable electronics: A review of materials, fabrication, devices, and applications. *Advanced Materials, 26*(31), 5310–5336. https://doi.org/10.1002/adma.201400633

Zhan, X., Si, C., Zhou, J., & Sun, Z. (2020). MXene and MXene-based composites: Synthesis, properties and environment-related applications. *Nanoscale Horizons, 5*(2), 235–258. https://doi.org/10.1039/c9nh00571d

Zheng, D., Hu, X., Lin, Y. S., & Chen, C. H. (2020). Tunable multi-resonance of terahertz metamaterial using split-disk resonators. *AIP Advances, 10*(12), Article 125305. https://doi.org/10.1063/1.5139263